Supporting Information

Accurately Predicting the Radiation Enhancement Factor in Plasmonic Optical Antenna-Emitters

Mao-Xin Zhang,[†,#] En-Ming You,[†,#] Peng Zheng,[‡] Song-Yuan Ding,[,†] Zhong-Qun Tian,[†] Martin Moskovits[§]*

[†] State Key Laboratory of Physical Chemistry of Solid Surfaces, Collaborative Innovation Center of Chemistry for Energy Materials, College of Chemistry and Chemical Engineering, Xiamen University, Xiamen 361005, China

[‡] School of Aerospace Engineering, Xiamen University, Xiamen 361005, China

[§] Department of Chemistry and Biochemistry, University of California, Santa Barbara, California, 93106, USA

[*]Corresponding Author: syding@xmu.edu.cn

Content

SI 1. Derivation of the rigorous ORT for three kinds of emitters: electric dipole, magnetic dipole, and electric quadrupole emitters

The rigorous optical reciprocity theorem (ORT)[1-3] is the theoretic basis of this article. We rewrote the forms of the ORT for three kinds of emitters, i.e., oscillating electric dipole, magnetic dipole, and electric quadrupole emitters, respectively.

We consider that the current density $\mathbf{J}_1(\mathbf{r})$ in volumes V_1 generates electric field $\mathbf{E}_1(\mathbf{r})$ and magnetic field $\mathbf{H}_1(\mathbf{r})$ in volumes V_2. Here V_1 and V_2 are spatially separate. We consider another current density $\mathbf{J}_2(\mathbf{r})$ in volumes V_2 generates electric field $\mathbf{E}_2(\mathbf{r})$ and magnetic field $\mathbf{H}_2(\mathbf{r})$ in volumes V_1. If both $\mathbf{J}_1(\mathbf{r})$ and $\mathbf{J}_2(\mathbf{r})$ are placed in the same medium with symmetric dielectric tensors, then $\mathbf{J}_1(\mathbf{r})$ and $\mathbf{E}_1(\mathbf{r})$, and $\mathbf{J}_2(\mathbf{r})$ and $\mathbf{E}_2(\mathbf{r})$ satisfy the following equation,

$$\int_{V_1} \mathbf{J}_1 \cdot \mathbf{E}_2 \mathrm{d}V = \int_{V_2} \mathbf{J}_2 \cdot \mathbf{E}_1 \mathrm{d}V \tag{1}$$

This is the integral form of the optical reciprocity theorem (ORT)[1, 3].

For an electric dipole emitter $\mathbf{p}_{\mathrm{e}}$ with subscript $i = 1$ or 2, the current densities are transformed to,

$$\mathbf{J}_1(\boldsymbol{r}) = -\mathrm{j}\omega \mathbf{p}_{\mathrm{ei}} \delta(\mathbf{r} - \mathbf{r}_{\mathrm{i}}) \tag{2}$$

Then equation (1) can be reduced to the simplified form,

$$\mathbf{p}_{\mathrm{e1}} \cdot \mathbf{E}_2(\mathbf{r}_1) = \mathbf{p}_{\mathrm{e2}} \cdot \mathbf{E}_1(\mathbf{r}_2) \tag{3}$$

which is the ORT form for oscillating electric dipole emitters.

The left-hand side of equation (1) can be further transformed into the case of an oscillating magnetic-dipole emitter $\mathbf{p}_{\mathrm{m}}$ or electric-quadrupole emitter with quadrupole tensor $Q_{\mathrm{ei},\rho\sigma}(i = 1,2;\ \rho,\sigma = 1,2,3)$,

$$\int_{V_1} \mathbf{J}_1 \cdot \mathbf{E}_2 dV = -\frac{\mathrm{j}\omega}{12}\left(\frac{\partial E_{2\rho}}{\partial x_\sigma} + \frac{\partial E_{2\sigma}}{\partial x_\rho}\right) Q_{\mathrm{e1},\rho\sigma} + \mathrm{j}\omega \mathbf{B}_2(\mathbf{r}_1) \cdot \mathbf{p}_{\mathrm{m1}} \tag{4}$$

Hence, we yield the ORT form for oscillating magnetic dipole emitters,

$$\mathbf{p}_{\mathrm{m}1} \cdot \mathbf{B}_2(\mathbf{r}_1) = \mathbf{p}_{\mathrm{m}2} \cdot \mathbf{B}_1(\mathbf{r}_2) \tag{5}$$

and ORT form for oscillating electric quadrupole emitters,

$$\left(\frac{\partial E_{2\rho}(\boldsymbol{r}_1)}{\partial x_\sigma} + \frac{\partial E_{2\sigma}(\boldsymbol{r}_1)}{\partial x_\rho}\right) Q_{\mathrm{e}1,\rho\sigma} = \left(\frac{\partial E_{1\rho}(\boldsymbol{r}_2)}{\partial x_\sigma} + \frac{\partial E_{1\sigma}(\boldsymbol{r}_2)}{\partial x_\rho}\right) Q_{\mathrm{e}2,\rho\sigma} \tag{6}$$

SI 2. Derivation of $G_2^{\mathrm{Exp}} = G_2^{\mathrm{Rec}}$ and $G_2^{\mathrm{Exp}} \approx G_2^{\mathrm{PW}}$ for emitters according to the ORT

As shown in Figure S1a, an emitter $\mathbf{p}_{\mathrm{loc}}^{\mathrm{Exp}}(\mathbf{r}_{\mathrm{m}}, \omega_{\mathrm{s}})$ is located at $\mathbf{r}_{\mathrm{m}}$ near the POA with a dipole moment p_0 along z axis. $\mathbf{p}_{\mathrm{loc}}^{\mathrm{Exp}}(\mathbf{r}_{\mathrm{m}}, \omega_{\mathrm{s}})$ and the generated electric field $\mathbf{E}_{\mathrm{far}}^{\mathrm{Exp}}(\mathbf{R}, \omega_{\mathrm{s}}, \mathbf{p}_{\mathrm{loc}}^{\mathrm{Exp}})$ at $\mathbf{R}$ where the detector is located are in the experimental configuration. $\mathbf{p}_{\mathrm{far}}^{\mathrm{Rec}}(\mathbf{R}, \omega_{\mathrm{s}})$, a dummy dipole with the same dipole moment p_0 at $\mathbf{R}$, and the generated electric field $\mathbf{E}_{\mathrm{loc}}^{\mathrm{Rec}}(\mathbf{r}_{\mathrm{m}}, \omega_{\mathrm{s}}, \mathbf{p}_{\mathrm{far}}^{\mathrm{Rec}})$ are in the reciprocal configuration.

The radiation enhancement G_2^{Exp} in the experimental configuration (Figure 1a) is

$$G_2^{\mathrm{Exp}}\left(\mathbf{R}, \omega_{\mathrm{s}}, \mathbf{p}_{\mathrm{loc}}^{\mathrm{Exp}}(\mathbf{r}_{\mathrm{m}})\right) = \left|\frac{\mathbf{E}_{\mathrm{far}}^{\mathrm{Exp}}\left(\mathbf{R}, \omega_{\mathrm{s}}, \mathbf{p}_{\mathrm{loc}}^{\mathrm{Exp}}\right)}{\mathbf{E}_{\mathrm{far,0}}^{\mathrm{Exp}}\left(\mathbf{R}, \omega_{\mathrm{s}}, \mathbf{p}_{\mathrm{loc}}^{\mathrm{Exp}}\right)}\right|^2 \tag{7}$$

$\mathbf{E}_{\mathrm{far}}^{\mathrm{Exp}}(\mathbf{R}, \omega_{\mathrm{s}}, \mathbf{p}_{\mathrm{loc}}^{\mathrm{Exp}})$ and $\mathbf{E}_{\mathrm{far,0}}^{\mathrm{Exp}}(\mathbf{R}, \omega_{\mathrm{s}}, \mathbf{p}_{\mathrm{loc}}^{\mathrm{Exp}})$ are generated by the $\mathbf{p}_{\mathrm{loc}}^{\mathrm{Exp}}(\mathbf{r}_{\mathrm{m}}, \omega_{\mathrm{s}})$ at the molecular position $\mathbf{r}_{\mathrm{m}}$ in the presence and absence of the POA nanostructure, respectively.

The local enhancement G_2^{Rec} in the reciprocal configuration (Figure 1c) is,

$$G_2^{\mathrm{Rec}}\left(\mathbf{r}_{\mathrm{m}}, \omega_{\mathrm{s}}, \mathbf{p}_{\mathrm{far}}^{\mathrm{Rec}}\right) = \left|\frac{\mathbf{E}_{\mathrm{loc}}^{\mathrm{Rec}}(\mathbf{r}_{\mathrm{m}}, \omega_{\mathrm{s}}, \mathbf{p}_{\mathrm{far}}^{\mathrm{Rec}})}{\mathbf{E}_{\mathrm{loc,0}}^{\mathrm{Rec}}(\mathbf{r}_{\mathrm{m}}, \omega_{\mathrm{s}}, \mathbf{p}_{\mathrm{far}}^{\mathrm{Rec}})}\right|^2 \tag{8}$$

where $\mathbf{E}_{\mathrm{loc}}^{\mathrm{Rec}}$ and $\mathbf{E}_{\mathrm{loc,0}}^{\mathrm{Rec}}$ are the electric field strength at $\mathbf{r}_{\mathrm{m}}$ with and without the POA nanostructure, respectively.

We should note that $\mathbf{E}_{\mathrm{far}}^{\mathrm{Exp}}$ and $\mathbf{E}_{\mathrm{far,0}}^{\mathrm{Exp}}$, $\mathbf{E}_{\mathrm{loc}}^{\mathrm{Rec}}$ and $\mathbf{E}_{\mathrm{loc,0}}^{\mathrm{Rec}}$, G_2^{Exp} and G_2^{Rec}, are dependent on the wavelength (i.e., angular frequency ω_{s}). For simplicity, we omit the ω_{s} in the following equations or expressions.

According to the rigorous ORT in equation (3), $\mathbf{E}_{\mathrm{far}}^{\mathrm{Exp}}(\mathbf{R}, \mathbf{p}_{\mathrm{loc}}^{\mathrm{Exp}})$ and $\mathbf{p}_{\mathrm{loc}}^{\mathrm{Exp}}(\mathbf{r}_{\mathrm{m}})$, and $\mathbf{E}_{\mathrm{loc}}^{\mathrm{Rec}}(\mathbf{r}_{\mathrm{m}}, \mathbf{p}_{\mathrm{far}}^{\mathrm{Rec}})$ and $\mathbf{p}_{\mathrm{far}}^{\mathrm{Rec}}(\mathbf{R})$ can be rigorously correlated by

$$\mathbf{E}_{\mathrm{far}}^{\mathrm{Exp}}\left(\mathbf{R}, \mathbf{p}_{\mathrm{loc}}^{\mathrm{Exp}}\right) \cdot \mathbf{p}_{\mathrm{far}}^{\mathrm{Rec}}(\mathbf{R}) = \mathbf{E}_{\mathrm{loc}}^{\mathrm{Rec}}\left(\mathbf{r}_{\mathrm{m}}, \mathbf{p}_{\mathrm{far}}^{\mathrm{Rec}}\right) \cdot \mathbf{p}_{\mathrm{loc}}^{\mathrm{Exp}}(\mathbf{r}_{\mathrm{m}}) \tag{9}$$

The $\mathbf{E}_{\mathrm{far}}^{\mathrm{Exp}}(\mathbf{R}, \mathbf{p}_{\mathrm{loc}}^{\mathrm{Exp}})$ generated by the $\mathbf{p}_{\mathrm{loc}}^{\mathrm{Exp}}(\mathbf{r}_{\mathrm{m}})$ can be decomposed into two perpendicular components, one component in the incident plane, and the other component perpendicular to the incident plane, which are denoted by the subscript '||' and '$\perp$', respectively. Aside from that, the $\mathbf{p}_{\mathrm{far}}^{\mathrm{Rec}}(\mathbf{R})$ can also be decomposed into two perpendicular directions as same as those of $\mathbf{E}_{\mathrm{far}}^{\mathrm{Exp}}$. Hence equation (7) can be transformed into two equations with the $\mathbf{p}_{\mathrm{loc,z}}^{\mathrm{Exp}}$ along z axis,

$$\mathbf{E}_{\mathrm{far},||}^{\mathrm{Exp}}(\mathbf{R}, \mathbf{p}_{\mathrm{loc,z}}^{\mathrm{Exp}}) \cdot \mathbf{p}_{\mathrm{far},||}^{\mathrm{Rec}}(\mathbf{R}) = \mathbf{E}_{\mathrm{loc,z}}^{\mathrm{Rec}}(\mathbf{r}_{\mathrm{m}}, \mathbf{p}_{\mathrm{far},||}^{\mathrm{Rec}}) \cdot \mathbf{p}_{\mathrm{loc,z}}^{\mathrm{Exp}} \tag{10}$$

$$\mathbf{E}_{\mathrm{far},\perp}^{\mathrm{Exp}}(\mathbf{R}, \mathbf{p}_{\mathrm{loc,z}}^{\mathrm{Exp}}) \cdot \mathbf{p}_{\mathrm{far},\perp}^{\mathrm{Rec}}(\mathbf{R}) = \mathbf{E}_{\mathrm{loc,z}}^{\mathrm{Rec}}\left(\mathbf{r}_{\mathrm{m}}, \mathbf{p}_{\mathrm{far},\perp}^{\mathrm{Rec}}\right) \cdot \mathbf{p}_{\mathrm{loc,z}}^{\mathrm{Exp}} \tag{11}$$

For the $\mathbf{p}_{\mathrm{loc,x}}^{\mathrm{Exp}}$ with the orientation along x-axis, equation (7) is transformed into the equations (12) and (13).

$$\mathbf{E}_{\mathrm{far},||}^{\mathrm{Exp}}(\mathbf{R}, \mathbf{p}_{\mathrm{loc,x}}^{\mathrm{Exp}}) \cdot \mathbf{p}_{\mathrm{far},||}^{\mathrm{Rec}}(\mathbf{R}) = \mathbf{E}_{\mathrm{loc,x}}^{\mathrm{Rec}}(\mathbf{r}_{\mathrm{m}}, \mathbf{p}_{\mathrm{far},||}^{\mathrm{Rec}}) \cdot \mathbf{p}_{\mathrm{loc,x}}^{\mathrm{Exp}} \tag{12}$$

$$\mathbf{E}_{\mathrm{far},\perp}^{\mathrm{Exp}}(\mathbf{R}, \mathbf{p}_{\mathrm{loc,x}}^{\mathrm{Exp}}) \cdot \mathbf{p}_{\mathrm{far},\perp}^{\mathrm{Rec}}(\mathbf{R}) = \mathbf{E}_{\mathrm{loc,x}}^{\mathrm{Rec}}\left(\mathbf{r}_{\mathrm{m}}, \mathbf{p}_{\mathrm{far},\perp}^{\mathrm{Rec}}\right) \cdot \mathbf{p}_{\mathrm{loc,x}}^{\mathrm{Exp}} \tag{13}$$

The in-plane radiation enhancement factor can be indirectly calculated by directly calculating the local-field enhancement factor in the reciprocal configuration.

$$G_{2,||}^{\mathrm{Exp}}\left(\mathbf{R}, \mathbf{p}_{\mathrm{loc,z}}^{\mathrm{Exp}}(\mathbf{r}_{\mathrm{m}})\right) = \frac{\mathbf{E}_{\mathrm{far},||}^{\mathrm{Exp}}(\mathbf{R},\mathbf{p}_{\mathrm{loc,z}}^{\mathrm{Exp}})}{\mathbf{E}_{\mathrm{far},||,0}^{\mathrm{Exp}}(\mathbf{R},\mathbf{p}_{\mathrm{loc,z}}^{\mathrm{Exp}})} = \frac{\mathbf{E}_{\mathrm{loc,z}}^{\mathrm{Rec}}(\mathbf{r}_{\mathrm{m}},\mathbf{p}_{\mathrm{far},||}^{\mathrm{Rec}})\cdot\mathbf{p}_{\mathrm{loc,z}}^{\mathrm{Exp}}/\mathbf{p}_{\mathrm{far},||}^{\mathrm{Rec}}(\mathbf{R})}{\mathbf{E}_{\mathrm{loc,z,0}}^{\mathrm{Rec}}(\mathbf{r}_{\mathrm{m}},\mathbf{p}_{\mathrm{far},||}^{\mathrm{Rec}})\cdot\mathbf{p}_{\mathrm{loc,z}}^{\mathrm{Exp}}/\mathbf{p}_{\mathrm{far},||}^{\mathrm{Rec}}(\mathbf{R})} \tag{14}$$

$$G_{2,||}^{\mathrm{Exp}}\left(\mathbf{R}, \mathbf{p}_{\mathrm{loc,z}}^{\mathrm{Exp}}(\mathbf{r}_{\mathrm{m}})\right) = \frac{\mathbf{E}_{\mathrm{far},||}^{\mathrm{Exp}}(\mathbf{R},\mathbf{p}_{\mathrm{loc,z}}^{\mathrm{Exp}})}{\mathbf{E}_{\mathrm{far},||,0}^{\mathrm{Exp}}(\mathbf{R},\mathbf{p}_{\mathrm{loc,z}}^{\mathrm{Exp}})} = \frac{\mathbf{E}_{\mathrm{loc,z}}^{\mathrm{Rec}}(\mathbf{r}_{\mathrm{m}},\mathbf{p}_{\mathrm{far},||}^{\mathrm{Rec}})}{\mathbf{E}_{\mathrm{loc,z,0}}^{\mathrm{Rec}}(\mathbf{r}_{\mathrm{m}},\mathbf{p}_{\mathrm{far},||}^{\mathrm{Rec}})} \tag{15}$$

Similarly, the out-of-plane radiation enhancement factor could be calculated as well,

$$G_{2,\perp}^{\mathrm{Exp}}\left(\mathbf{R}, \mathbf{p}_{\mathrm{loc,z}}^{\mathrm{Exp}}(\mathbf{r}_{\mathrm{m}})\right) = \frac{\mathbf{E}_{\mathrm{far},\perp}^{\mathrm{Exp}}(\mathbf{R},\mathbf{p}_{\mathrm{loc,z}}^{\mathrm{Exp}})}{\mathbf{E}_{\mathrm{far},\perp,0}^{\mathrm{Exp}}(\mathbf{R},\mathbf{p}_{\mathrm{loc,z}}^{\mathrm{Exp}})} = \frac{\mathbf{E}_{\mathrm{loc,z}}^{\mathrm{Rec}}(\mathbf{r}_{\mathrm{m}},\mathbf{p}_{\mathrm{far},\perp}^{\mathrm{Rec}})}{\mathbf{E}_{\mathrm{loc,z,0}}^{\mathrm{Rec}}(\mathbf{r}_{\mathrm{m}},\mathbf{p}_{\mathrm{far},\perp}^{\mathrm{Rec}})} \tag{16}$$

As a result, we obtain the important equation,

$$G_{2}^{\mathrm{Exp}}\left(\mathbf{R}, \mathbf{p}_{\mathrm{loc}}^{\mathrm{Exp}}(\mathbf{r}_{\mathrm{m}})\right) = G_{2}^{\mathrm{Rec}}\left(\mathbf{r}_{\mathrm{m}}, \mathbf{p}_{\mathrm{far}}^{\mathrm{Rec}}(\mathbf{R})\right) \tag{17}$$

If the distance between $\mathbf{p}_{\text{loc}}^{\text{Exp}}$ and $\mathbf{E}_{\text{far}}^{\text{Exp}}$, i.e., R is sufficiently large ($|\mathbf{r}_{\text{m}}| \ll R$), the field $\mathbf{E}_{\text{loc,z,0}}^{\text{Rec}}$ in the absence of POAs can be approximated by expanding the free-space dipole field[2],

$$\mathbf{E}_{\text{loc,z,0}}^{\text{Rec}}(\mathbf{r}_{\text{m}}) \approx E_{\text{p}} \mathbf{e}_{\text{loc}}^{\text{Rec}} e^{-\text{j}\mathbf{k}_{\mathbf{R}} \cdot \mathbf{r}_{\text{m}}} \tag{18}$$

with $E_{\text{p}} = \frac{k_R^2 p_{\text{far}}^{\text{Rec}} e^{\text{j}k_{\mathbf{R}}R}}{4\pi\varepsilon_0\varepsilon_{\text{s}}R}$. The right-hand side of the approximate equation is the electric field $\mathbf{E}_{\text{loc,z,0}}^{\text{PW}}$ of a plane wave (PW), including propagating wavevector $\mathbf{k}_{\mathbf{R}}$ along $-\mathbf{R}$ direction, the complex amplitude E_{p} and polarization $\mathbf{e}_{\text{loc}}^{\text{Rec}}$. In other word, $\mathbf{E}_{\text{loc,z,0}}^{\text{Rec}}$ is the approximate quantity to $\mathbf{E}_{\text{loc,z,0}}^{\text{PW}}$.

Similarly, in the presence of the POA, $\mathbf{E}_{\text{loc,z}}^{\text{Rec}}(\mathbf{r}_{\text{m}})$ is the approximate quantity to $\mathbf{E}_{\text{loc,z}}^{\text{PW}}(\mathbf{r}_{\text{m}})$, according to the equation (9),

$$\mathbf{e}_{\text{loc}}^{\text{Exp}} \cdot \mathbf{E}_{\text{loc,z}}^{\text{Rec}}(\mathbf{r}_{\text{m}}) \approx \frac{E_{\text{p}}}{p_{\text{far}}^{\text{Rec}}} p_{\text{loc}}^{\text{Exp}} \frac{\mathbf{e}_{\text{loc}}^{\text{Rec}} \cdot \mathbf{E}_{\text{loc,z}}^{\text{PW}}}{E_{\text{p}}} \tag{19}$$

Similar to equations (14) and (15), we can define two plane waves with two perpendicular polarizations as those of the dipole $\mathbf{p}_{\text{far}}^{\text{Rec}}(\mathbf{R})$ with the subscript '||' and '$\perp$' respectively. Hence, we deduce

$$\frac{\mathbf{E}_{\text{loc,z}}^{\text{Rec}}\left(\mathbf{r}_{\text{m}}, \mathbf{p}_{\text{far,||}}^{\text{Rec}}\right)}{\mathbf{E}_{\text{loc,z,0}}^{\text{Rec}}\left(\mathbf{r}_{\text{m}}, \mathbf{p}_{\text{far,||}}^{\text{Rec}}\right)} \approx \frac{\mathbf{E}_{\text{loc,z}}^{\text{PW,||}}(\mathbf{r}_{\text{m}})}{\mathbf{E}_{\text{loc,z,0}}^{\text{PW,||}}(\mathbf{r}_{\text{m}})} \tag{20}$$

$$\frac{\mathbf{E}_{\text{loc,z}}^{\text{Rec}}\left(\mathbf{r}_{\text{m}}, \mathbf{p}_{\text{far,}\perp}^{\text{Rec}}\right)}{\mathbf{E}_{\text{loc,z,0}}^{\text{Rec}}\left(\mathbf{r}_{\text{m}}, \mathbf{p}_{\text{far,}\perp}^{\text{Rec}}\right)} \approx \frac{\mathbf{E}_{\text{loc,z}}^{\text{PW,}\perp}(\mathbf{r}_{\text{m}})}{\mathbf{E}_{\text{loc,z,0}}^{\text{PW,}\perp}(\mathbf{r}_{\text{m}})} \tag{21}$$

Combining equations (17)-(20), we can deduce,

$$G_2^{\text{Exp}}\left(\mathbf{R}, \mathbf{p}_{\text{loc}}^{\text{Exp}}(\mathbf{r}_{\text{m}})\right) = G_2^{\text{Rec}}\left(\mathbf{r}_{\text{m}}, \mathbf{p}_{\text{far}}^{\text{Rec}}(\mathbf{R})\right) \approx G_2^{\text{PW}}(\mathbf{r}_{\text{m}}, \mathbf{k}_{\mathbf{R}}) \tag{22}$$

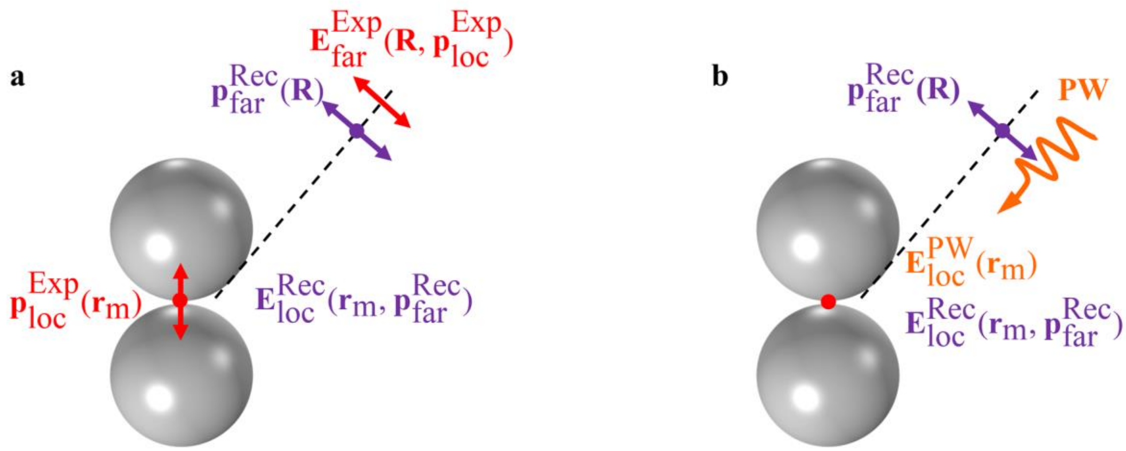

Figure S1. Schematics of the rigorous and approximate ORT. (a) The electric field $\mathbf{E}_{\text{far}}^{\text{Exp}}(\mathbf{R}, \mathbf{p}_{\text{loc}}^{\text{Exp}})$ at $\mathbf{R}$ generated by an oscillating electric dipole $\mathbf{p}_{\text{loc}}^{\text{Exp}}(\mathbf{r}_{\text{m}})$ at $\mathbf{r}_{\text{m}}$ (double-headed red arrow with a red circle) in the experimental configuration and $\mathbf{E}_{\text{loc}}^{\text{Rec}}\left(\mathbf{r}_{\text{m}}, \mathbf{p}_{\text{far}}^{\text{Rec}}(\mathbf{R})\right)$ at $\mathbf{r}_{\text{m}}$ generated by an oscillating electric dipole $\mathbf{p}_{\text{far}}^{\text{Rec}}(\mathbf{R})$ at $\mathbf{R}$ (double-headed purple arrow with a purple circle) in the reciprocal configuration are exactly correlated according to the rigorous ORT in equation (3). (b) The electric field $\mathbf{E}_{\text{loc}}^{\text{PW}}$ at $\mathbf{r}_{\text{m}}$ generated by a plane wave (PW, orange) is approximately correlated to $\mathbf{E}_{\text{loc}}^{\text{Rec}}$ generated by $\mathbf{p}_{\text{far}}^{\text{Rec}}(\mathbf{R})$ according to the approximate ORT in equation (22). The POA consists of a Ag nanosphere dimer. The electric field $\mathbf{E}_{\text{far}}^{\text{Exp}}$ and $\mathbf{E}_{\text{loc}}^{\text{Rec}}$ are wavelength dependent, and the frequency of scattering light ω_{s} is omitted here.

The magnetic dipole $\mathbf{p}_{\text{m}}(\mathbf{R})$ along the y-axis was chosen in this article, and thus we only consider the magnetic flux density $\mathbf{B}_{\text{y}}$ along the y-axis in the simulations. We can derive equation (17) for the oscillating magnetic dipolar emitter by replacing $\mathbf{E}$ with $\mathbf{B}$ and replacing $\mathbf{p}_{\text{e}}$ with $\mathbf{p}_{\text{m}}$ according to equation (5).

In the simplest electric quadrupole $\overleftrightarrow{\mathbf{Q}}_{\text{e},11}$, the charges are distributed as '+, −, −, +' along the x-axis, where '+' represents a positive elementary charge and '−' represents a negative elementary charge, and the subscript '11' denotes the $\mathbf{e}_{\text{x}}\mathbf{e}_{\text{x}}$ component of the quadrupole tensor. We chose $\overleftrightarrow{\mathbf{Q}}_{\text{e},11}$ as the electric quadrupole emitter in this article. We consider only the x-direction gradient of the electric field along the z-axis $\partial\mathbf{E}_{\text{z}}/\partial x$ in this article to derive the equation (17) for the electric quadrupolar emitter by replacing $\mathbf{E}$ with $\partial\mathbf{E}_{\text{z}}/\partial x$ according to equation (6).

SI 3. Numerical demonstration of the equivalence between G_2^{Exp} and G_2^{Rec} for electric dipole emitters in three classical plasmonic optical antenna systems

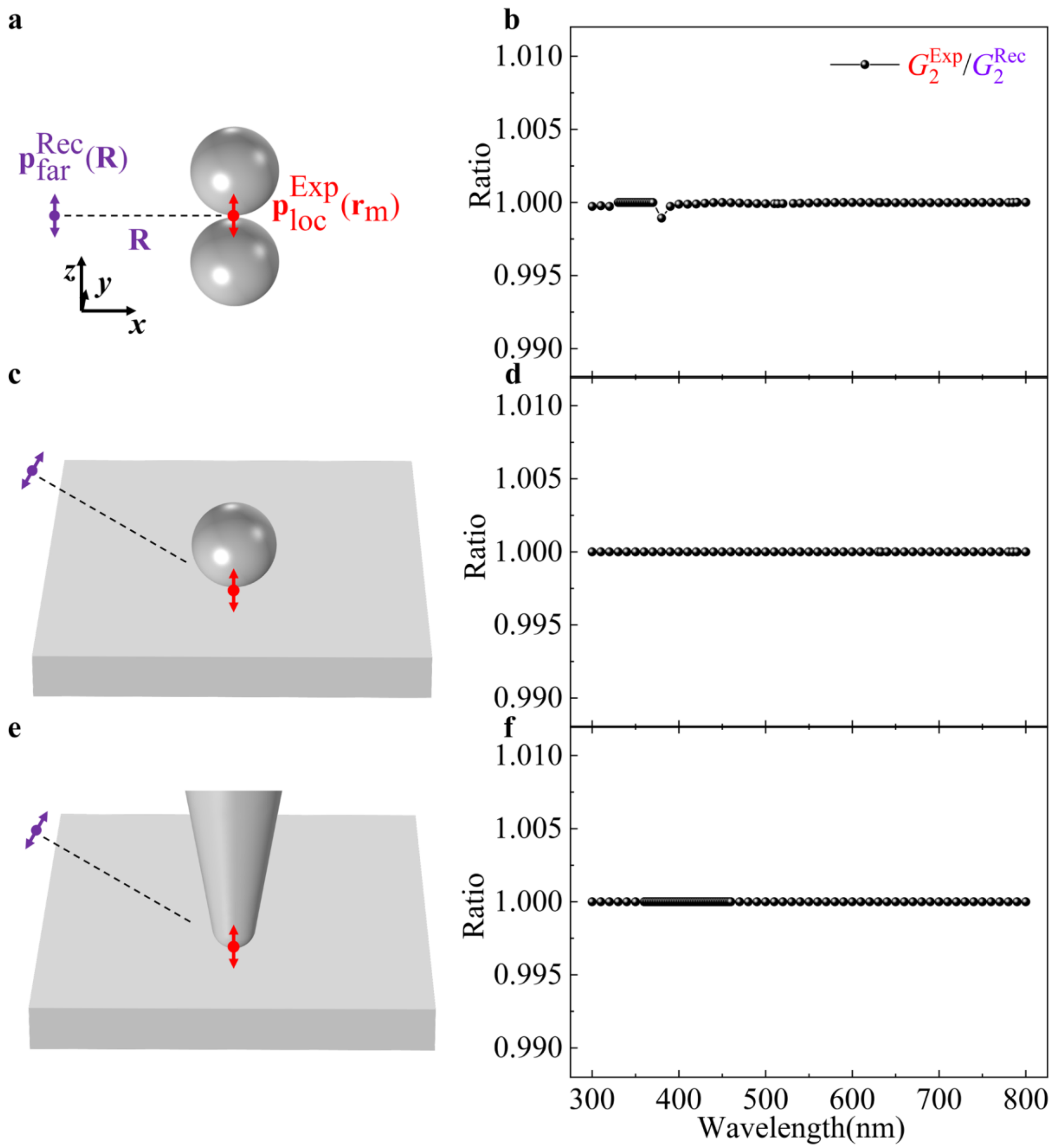

Figure S2. Comparison of G_2^{Exp} and G_2^{Rec} for oscillating electric dipolar emitters in three classical plasmonic optical antenna (POA) systems. (a) Diagram of POA-I: Ag nanosphere dimer (diameter of each sphere is 50 nm, inter-particle gap size is 2 nm) excited by an oscillating electric dipole emitter $\mathbf{p}_{\mathrm{loc}}^{\mathrm{Exp}}$ (double-headed arrow in red color) in the experimental configuration and $\mathbf{p}_{\mathrm{far}}^{\mathrm{Rec}}$ (double-headed arrow in purple color) at the distance R =900 nm in the reciprocal configuration, and the radius of the solution domain is 1 μm. (b) Wavelength-dependent ratio $G_2^{\text{Exp}}/G_2^{\text{Rec}}$ in (a). (c) Diagram of POA-II: Ag nanosphere coupled with a Ag substrate (diameter of sphere is 150 nm, inter-particle gap size is 4 nm, R is 1.15 μm, and radius of the solution domain is 1.2 μm). (d) Wavelength-dependent ratio $G_2^{\text{Exp}}/G_2^{\text{Rec}}$ in (c). (e) Diagram of POA-III: Ag scanning probe coupled with an Ag substrate (radius of curvature of the probe is 25 nm, probe length is1.2 μm, angle of cone of the probe is 20º, probe-substrate gap size is 2 nm, R is 1.15 μm, and radius of the solution domain is 1.2 μm). (f) Wavelength-dependent ratio $G_2^{\text{Exp}}/G_2^{\text{Rec}}$ in (e). The ratio $G_2^{\text{Exp}}/G_2^{\text{Rec}}$ in b, d, and f are close to one with the maximum relative errors 0.03%, 0, and 0, respectively, for λ in the range of 300 to 800 nm. The oscillating electric dipolar source is defined by the built-in function in the COMSOL software. The solution to G_2^{Exp} and G_2^{Rec} in this model is obtained by solving Maxwell's equations in the absorbing boundary condition with the point source $\mathbf{p}_{\text{far}}^{\text{Rec}}$ in the solution domain. The dipolar emitter $\mathbf{p}_{\text{loc}}^{\text{Exp}}$ in the experimental configuration is located in the gap of the POA, and the dipolar emitter $\mathbf{p}_{\text{far}}^{\text{Rec}}$ in the reciprocal configuration is located in $\mathbf{R}$.

SI 4. Definition of the analytical background field

In this article, the surrounding environment of the simulations is vacuum with the refractive index $n_0 = 1$, permittivity ε_0 and permeability μ_0. We defined the background fields of all the emitters analytically.

(1) Source 1: Oscillating electric dipolar emitter

The analytic form of an oscillating electric dipolar emitter $\mathbf{p}_{\mathrm{far}}^{\mathrm{Rec}}(R, \theta, \varphi)$ can be obtained from Jackson's book on *Electrodynamics*.[4] We set $\varphi = 0^{\circ}$ for the polarization of the dipole to be parallel to the XOZ-plane, $\theta = 60^{\circ}$. The position of the dipole in the rectangular coordinate system is (x_0, 0, z_0) where $x_0 = -R\sin(\theta)$, $z_0 = R\cos(\theta)$. The electric dipolar moment along *z*-axis is denoted by $\mathbf{p}_{\mathrm{z}}$.

If the length of the dipole is much smaller than the wavelength, the vector potential **A** can be described as

$$\mathbf{A} = \mathbf{e}_{\mathrm{z}} \frac{\mu_0 \dot{\mathbf{p}}_{\mathrm{z}}}{4\pi r} e^{-\mathrm{j}\mathbf{k}\cdot\mathbf{r}} \tag{23}$$

The magnetic field **H** and the electric field **E** can be deduced by

$$\mathbf{H} = \frac{1}{\mu_0} \nabla \times \mathbf{A} \tag{24}$$

$$\mathbf{E} = \frac{1}{j\omega\varepsilon_0} \nabla \times \mathbf{H} \tag{25}$$

We performed the rotation operations twice and translation operation once, to ensure that the direction of $\mathbf{p}_{\mathrm{far}}^{\mathrm{Rec}}(R, \theta, \varphi)$ is same as the polarization of the PW. Hence, the analytical form of $\mathbf{p}_{\mathrm{far}}^{\mathrm{Rec}}(R, \theta, \varphi)$ at any distant positions at R can be defined.

The analytical form of the electric field generated by $\mathbf{p}_{\mathrm{far}}^{\mathrm{Rec}}(R, \theta, \varphi)$ is set as the background field to solve the electric field distribution with or without any POAs.

The parameters of $\mathbf{p}_{\text{far}}^{\text{Rec}}$ set in COMSOL is shown in the following. (x0, y0, z0) is the position parameter of $\mathbf{p}_{\text{far}}^{\text{Rec}}$. The following parameters is set in variables' part of definitions' section in COMSOL.

"x1 = cos(theta) * (x - x0) - sin(theta) * (z - z0);

y1 = y - y0;

z1 = sin(theta) * (x - x0) + cos(theta) * (z - z0);

rdp = sqrt((x1)^2 + (y1)^2 + (z1)^2);

phi_0 = (y1==0) * (x1>=0) * (0[rad]) + (x1>0) * (y1>0) * atan(y1/x1) + (y1>0) * (x1==0) * pi/2 + (x1<0) * (y1>0) * (atan(y1/x1) + pi[rad]) + (y1==0) * (x1<0) * (pi[rad]) + (x1==0) * (y1<0) * (3/2 * pi[rad]) + (x1<0) * (y1<0) * (atan(y1/x1) + pi[rad]) + (x1>0) * (y1<0) * (atan(y1/x1) + 2 * pi[rad]);

theta_0 = acos((z1)/rdp);

Vm = p0 / (4 * pi * epsilon0_const), where p0 is the value of the electric dipolar moment;

Ph = -j * ewfd.k0 * na * rdp, where na is the refractive index of the environment;

Er = 2 * Vm * cos(theta_0) * (Ph-1) * exp(Ph) / rdp^3;

Etheta = Vm * sin(theta_0) * ((ewfd.k0 * na * rdp)^2 + Ph - 1) * exp(Ph) / rdp^3**;**

Ephi = 0 [V/m];

Ex1 = Er * sin(theta_0) * cos(phi_0) + Etheta * cos(theta_0) * cos(phi_0) - Ephi * sin(phi_0);

Ey1 = Er * sin(theta_0) * sin(phi_0) + Etheta * cos(theta_0) * sin(phi_0) + Ephi * cos(phi_0);

Ez1 = Er * cos(theta_0) - Etheta * sin(theta_0);

Ex0 = Ex1 * cos(theta) + Ez1 * sin(theta);

Ey0 = Ey1;

Ez0 = - Ex1 * sin(theta) + Ez1 * cos(theta)".

(2) Source 2: Oscillating magnetic dipolar emitter

We choose an oscillating magnetic dipolar emitter $\mathbf{p}_{\mathrm{m}}(\mathbf{r}_{\mathrm{m}})$ along y axis at $\mathbf{r}_{\mathrm{m}}$ to study the radiation enhancement. The polarization is perpendicular to the XOZ plane. The magnetic dipolar moment is denoted by $\mathbf{p}_{\mathrm{m}}$.

The vector potential $\mathbf{A}$ can be described as

$$\mathbf{A} = \frac{ik\mu_0 e^{-\mathrm{j}\mathbf{k}\cdot\mathbf{r}}}{4\pi r}\mathbf{e}_{\mathrm{r}} \times \mathbf{p}_{\mathrm{m}} \tag{26}$$

We can acquire magnetic field strength $\mathbf{H}_1$ and electric field strength $\mathbf{E}_1$ according to equations (24) and (25) and perform the translation operation once to obtain the analytical form of the electric field, which is generated by $\mathbf{p}_{\mathrm{m}}^{\mathrm{Rec}}(\mathbf{R})$ at any distant position $\mathbf{R}$.

The analytical form of the electric field generated by $\mathbf{p}_{\mathrm{m}}^{\mathrm{Rec}}(R,\theta,\varphi)$ is set as the background field to solve the electric field distribution with or without the POA-II.

The parameters of $\mathbf{p}_{\mathrm{m}}^{\mathrm{Rec}}$ set in COMSOL is shown in the following. (x0, y0, z0) is the position parameter of $\mathbf{p}_{\mathrm{m}}^{\mathrm{Rec}}$. The following parameters is set in variables' part of definitions' section in COMSOL.

"x1 = x - x0;

y1 = y - y0;

z1 = z - z0;

rdp = sqrt((x1)^2 + (y1)^2 + (z1)^2);

phi_0 = (y1==0) * (x1>=0) * (0[rad]) + (x1>0) * (y1>0) * atan(y1/x1) + (y1>0) * (x1==0) * pi/2 + (x1<0) * (y1>0) * (atan(y1/x1) + pi[rad]) + (y1==0) * (x1<0) * (pi[rad]) + (x1==0) * (y1<0) * (3/2 * pi[rad]) + (x1<0) * (y1<0) * (atan(y1/x1) + pi[rad]) + (x1>0) * (y1<0) * (atan(y1/x1) + 2 * pi[rad]);

theta_0 = acos((z1)/rdp);

Vm = ewfd.k0 * pm0 / (4 * pi * epsilon0_const * ewfd.omega) * exp(-1i * ewfd.k0 * na * rdp) , where na is the environmental refractive index and pm0 is the value of the magnetic dipolar moment;

Ph = ewfd.k0^2 / rdp – 2 / rdp^3;

Er = 0[V/m];

Etheta = Vm * cos(phi_0) * (- Ph);

Ephi = Vm * cos(theta_0) * sin(phi_0) * Ph;

Ex0 = Er * sin(theta_0) * cos(phi_0) + Etheta * cos(theta_0) * cos(phi_0) - Ephi * sin(phi_0);

Ey0 = Er * sin(theta_0) * sin(phi_0) + Etheta * cos(theta_0) * sin(phi_0) + Ephi * cos(phi_0);

Ez0 = Er * cos(theta_0) - Etheta * sin(theta_0)”.

(3) Source 3: Oscillating electric quadrupolar emitter

We choose an oscillating electric quadrupole $\overleftrightarrow{\mathbf{Q}}_{\mathrm{e},11}(\mathbf{r}_{\mathrm{m}})$ along to $\mathbf{e}_{\mathrm{x}}\mathbf{e}_{\mathrm{x}}$ to study the radiation enhancement. The electric quadrupolar tensor is denoted by $\overleftrightarrow{\mathbf{Q}}_{\mathrm{e},11}$.

The vector potential $\mathbf{A}$ can be described as

$$\mathbf{A} = -\frac{ik\mu_0 e^{-\mathbf{jk}\cdot\mathbf{r}}}{24\pi r}\mathbf{e}_{\mathrm{r}} \cdot \dot{\overleftrightarrow{\mathbf{Q}}}_{\mathrm{e},11} \tag{27}$$

We can acquire $\mathbf{H}_1$ and $\mathbf{E}_1$ according to equations (24) and (25) perform the translation operation once to translate the coordinate system of $\overleftrightarrow{\mathbf{Q}}_{\mathrm{e},11}(\mathbf{r}_{\mathrm{m}})$ to that of $\overleftrightarrow{\mathbf{Q}}_{\mathrm{e},11}(\mathbf{R})$ and to obtain the analytical electric field $\mathbf{E}_{\mathrm{Q}}$ generated by $\overleftrightarrow{\mathbf{Q}}_{\mathrm{e},11}(\mathbf{R})$ in the coordinate system of $\overleftrightarrow{\mathbf{Q}}_{\mathrm{e},11}(\mathbf{R})$.

The analytical form of the electric field generated by $\overleftrightarrow{\mathbf{Q}}_{\mathrm{e},11}(\mathbf{R})$ is set as the background field to solve the electric field distribution with or without the POA-II.

The parameters of $\overleftrightarrow{\mathbf{Q}}_{\mathrm{e},11}$ set in COMSOL is shown in the following. (x0, y0, z0) is the middle point-position parameter of $\overleftrightarrow{\mathbf{Q}}_{\mathrm{e},11}$. The following parameters is set in variables' part of definitions' section in COMSOL.

“x1 = x - x0;

y1 = y - y0;

z1 = z - z0;

rdp = sqrt((x1)^2 + (y1)^2 + (z1)^2);

phi_0 = (y1==0) * (x1>=0) * (0[rad]) + (x1>0) * (y1>0) * atan(y1/x1) + (y1>0) * (x1==0) * pi/2 + (x1<0) * (y1>0) * (atan(y1/x1) + pi[rad]) + (y1==0) * (x1<0) * (pi[rad]) + (x1==0) * (y1<0)

* (3/2 * pi[rad]) + (x1<0) * (y1<0) * (atan(y1/x1) + pi[rad]) + (x1>0) * (y1<0) * (atan(y1/x1) + 2 * pi[rad]);

theta_0 = acos((z1)/rdp);

Ck = - ewfd.k0^4 * dp0 / (24 * pi * epsilon0_const), where dp0 is the value of a dipolar moment in the electric quadrupole;

Fr0 = ewfd.k0 * na * rdp;

Ep = exp(-j*Fr0);

Fr1 = (-1 / Fr0^2 + 2 * j / Fr0^3) * Ep;

Fr2 = (i / Fr0 + 2 / Fr0^2 – 2 * j / Fr0^3) * Ep;

Er = Ck * Fr1 * ((2 * cos(theta_0)^2 - sin(theta_0)^2 - 1) * cos(phi_0)^2 + sin(phi_0)^2);

Etheta = - Ck * Fr2 * (sin(theta_0) * cos(theta_0) * cos(phi_0)^2)**;**

Ephi = Ck * Fr2 * (sin(theta_0) * cos(phi_0) * sin(phi_0));

Ex0 = Er * sin(theta_0) * cos(phi_0) + Etheta * cos(theta_0) * cos(phi_0) - Ephi * sin(phi_0);

Ey0 = Er * sin(theta_0) * sin(phi_0) + Etheta * cos(theta_0) * sin(phi_0) + Ephi * cos(phi_0);

Ez0 = Er * cos(theta_0) - Etheta * sin(theta_0)”.

(4) Source 4: PW

The analytical form of the electric field of a PW, i.e., $\mathbf{E} = E_0 e^{-\mathrm{j}\mathbf{k}\cdot\mathbf{r}}$, where $E_0 = 1\ \mathrm{V/m}$, and **k** and **r** represent the propagating wavevector of the PW and the space coordinate, respectively, was set as the background field of the PW to solve the electric field distribution with or without any POAs.

SI 5. Single point $G_2^{\mathrm{PW}}/G_2^{\mathrm{Rec}}$ in three typical E-POA systems

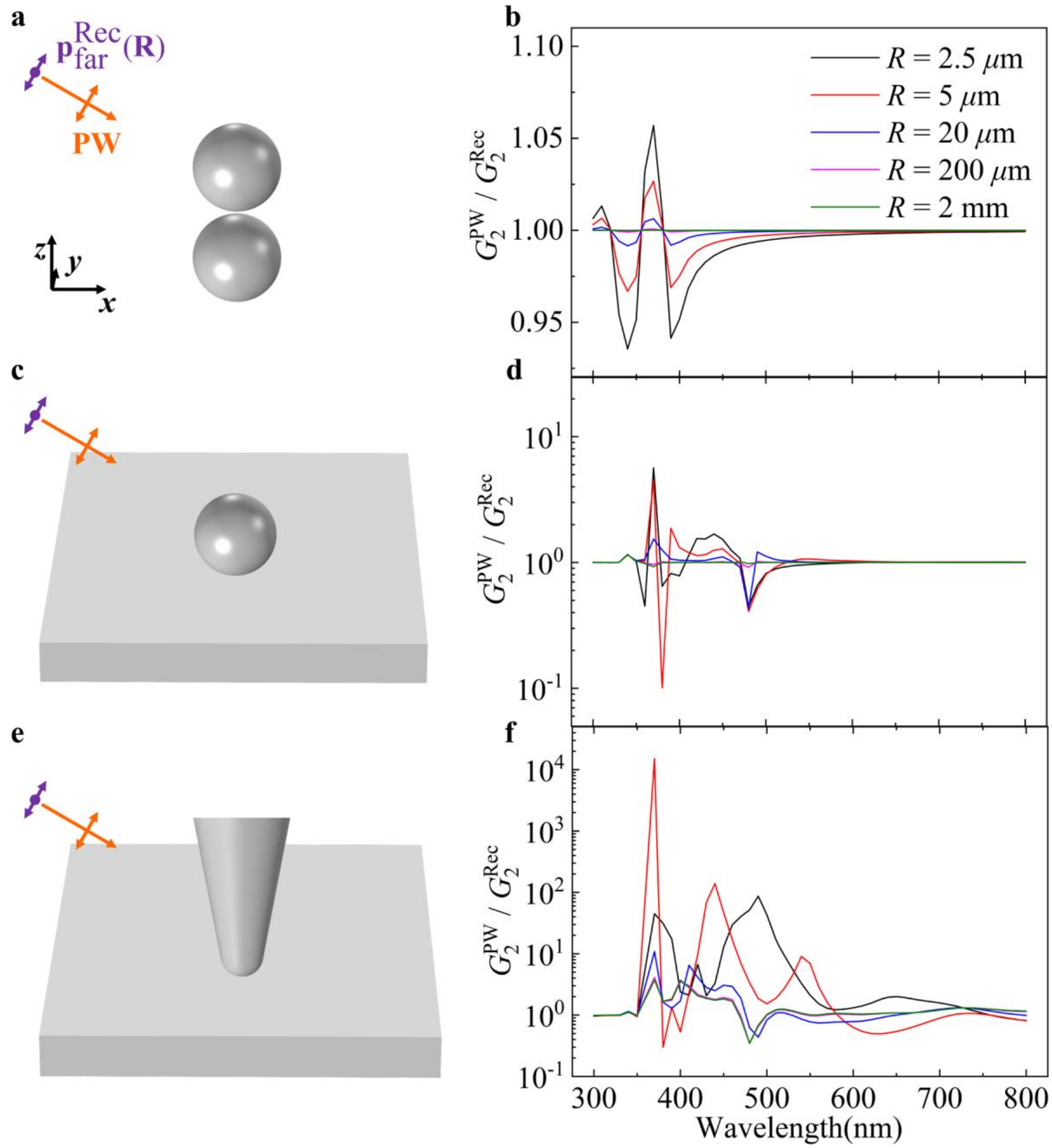

Figure S3. Comparison of the single-point radiation enhancement factors G_2^{PW} and G_2^{Rec} in three typical E-POA systems. (a) Diagram of POA-I: Ag nanosphere dimer (diameter is 100 nm and inter-particle gap size is 2 nm) excited by a PW in a PWA configuration (orange arrow) and an oscillating electric dipole $\mathbf{p}_{\mathrm{far}}^{\mathrm{Rec}}$ (purple double-headed arrow) at $\mathbf{R}$ in a reciprocal configuration. The incident angle is 60° to the normal with p polarization. The model is surrounded by a perfectly matched layer. (b) Calculated wavelength-dependent ratio $G_2^{\mathrm{PW}}/G_2^{\mathrm{Rec}}$ of POA-I with R varied from 2.5 μm to 2 mm. (c-d) Same as (a-b) but POA-II: Ag nanosphere (diameter is 100 nm) coupling with a Ag substrate. The particle-substrate gap size is 2 nm. (e-f) Same as (a-b) but POA-

III: Ag scanning probe coupling with an Ag substrate. Geometric parameters of the scanning probe: radius of curvature is 25 nm, length is 1.75 μm, angle of cone is 20º, probe-substrate gap is 2 nm. The radius of the substrate is 1.75 μm in the latter two systems. The position of a single point for analyzing $G_2^{\mathrm{PW}}/G_2^{\mathrm{Rec}}$ in (a) is located at the center of the gap.

SI 6. The detailed parameters in simulations

Maxwell's equations are solved by finite element method with a commercial software COMSOL Multiphysics. For POA-I system in Figure 2a, the maximum free triangular mesh size on the surface of each nanosphere is 2 nm, the mesh size in the middle of the inter-particle gap is 0.5 nm and the thickness of the perfect matched layer (PML) is 400 nm. The diameter of solution domain which does not include the thickness of PML is 2 μm.

For POA-II system in Figure 2d, the nanosphere is rotated 45 degree along y-axis and the maximum free triangular mesh size of the 1/4 surface of the sphere which is near the flat substrate surface is 1 nm. The mesh size of other part of the sphere is 5 nm, and the thickness of the perfect matched layer (PML) is 300 nm. The diameter of solution domain is 3.5 μm.

For POA-III system in Figure 2g, the maximum free triangular mesh size of the surface of the probe apex is 1 nm and the thickness of the perfect matched layer (PML) is 300 nm. The diameter of solution domain is 3.5 μm. The symmetric boundary condition called Perfect Magnetic Conductor in x-z plane is used for decreasing the complexity.

For magnetic dipole system in Figure 3a and electric quadrupole system in Figure 3d, the mesh size and the thickness of PML are the same as those of POA-II system in Figure 2d. The diameter of solution domain in the former two systems is 2.4 μm and the full model is used because the background field of magnetic dipole and electric quadrupole is not symmetric.

A 0.8 nm-radius sphere is set in the middle of the nanogap between the particle or probe and the flat substrate to refine the mesh grid of which the size ranges from 0.1 nm to 0.2 nm in all models. All the solution domain is set as a sphere.

A perfect matched layer (PML) outside the solution domain is set in all models to simulate an open and reflection-free boundary. The lower hemisphere is the substrate except for POA-I in Figure 2a and the probe is tangent to the upper hemisphere for POA-III in Figure 2g. Each emitter with position R varied from 2.5 μm to 2 mm in our model is outside the PML and the specific electric field of each emitter is set as the background field to excite the whole system which is kept at the same size.

SI 7. Near-field modes of a PW with different incident angles in POA-II

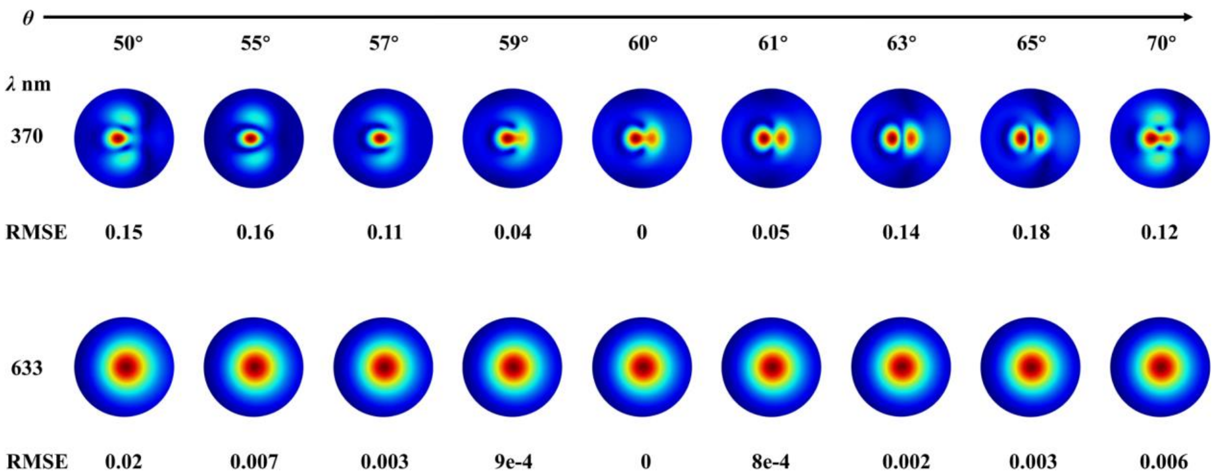

Figure S4. Near-field distribution ($|\mathbf{E}_z|/|\mathbf{E}_{z,\max}|$) in the POA-II system excited by a PW with incident angle θ varied from 50° to 70° along the z-axis at $\lambda = 370$ nm or $\lambda = 633$ nm. The corresponding RMSE value are shown in the following row. High-order plasmonic modes in POA-II system excited by a PW at $\lambda = 370$ nm are sensitive to the incident angle θ varied from 50° to 70° of the PW, and low-order plasmonic modes at $\lambda = 633$ nm remain almost unchanged with θ varied from 50° to 70°.

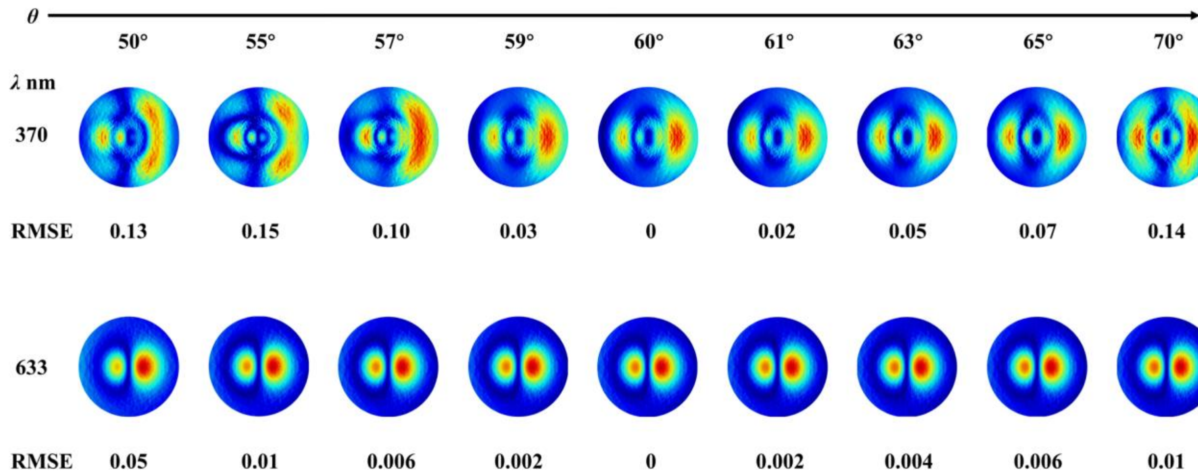

Figure S5. Near-field distribution ($|\mathbf{E}_{\mathrm{x}}|/|\mathbf{E}_{\mathrm{x,max}}|$) in the POA-II system excited by a PW with incident angle θ varied from 50° to 70° along the z-axis at $\lambda = 370$ nm or $\lambda = 633$ nm. The corresponding RMSE value are shown in the following row. High-order plasmonic modes in POA-II system excited by a PW at $\lambda = 370$ nm are sensitive to the incident angle θ varied from 50° to 70° of the PW, and low-order plasmonic modes at $\lambda = 633$ nm remain almost unchanged with θ varied from 50° to 70°.

SI 8. Radiative pattern of an oscillating electric dipole and a PW before interacting with POA-II

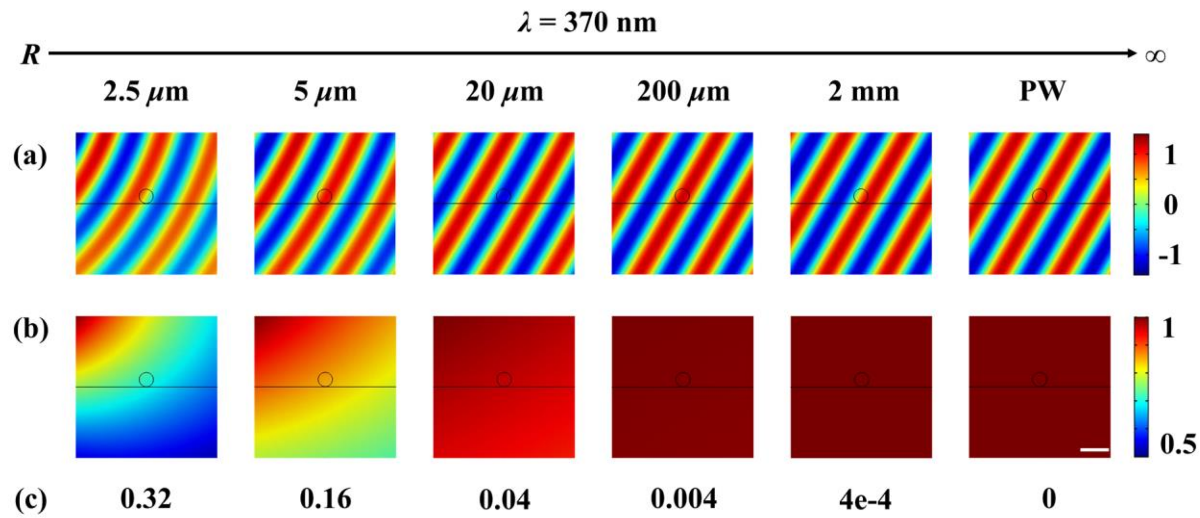

Figure S6. Diagrams of different radiative patterns generated by an oscillating electric dipole with varied R and a PW at $\lambda = 370$ nm, respectively. The distribution of (a) the normalized background electric field E_{bz} along the z-axis $\mathbf{E}_{\text{bz}}/\mathbf{E}_{\text{bz,max}}$ (including the phase) and that of (b) the normalized amplitude $|\mathbf{E}_{\text{bz}}|/|\mathbf{E}_{\text{bz,max}}|$ in 1 μm × 1 μm area becomes more similar to the PW as R increases from 2.5 μm to 2 mm. The black line shows the boundary of a nanosphere and the interface between the air and silver substrate. The RMSE between $|\mathbf{E}_{\text{bz}}(R)|/|\mathbf{E}_{\text{bz,max}}(R)|$ and $|\mathbf{E}_{\text{bz}}(\text{PW})|/|\mathbf{E}_{\text{bz,max}}(\text{PW})|$ are shown in (c). The wave front of the dipole is curving and that of the PW is straight when R is 2.5 μm or 5 μm. However, the wave front of the dipole becomes straight and similar to the PW when R becomes larger. The white scale bar is 0.2 μm.

SI 9. Discussion of effects of dipole direction in POA-II-$\mathbf{p}_{\mathrm{loc,x}}^{\mathrm{Exp}}$ and POA-III-$\mathbf{p}_{\mathrm{loc,x}}^{\mathrm{Exp}}$ systems

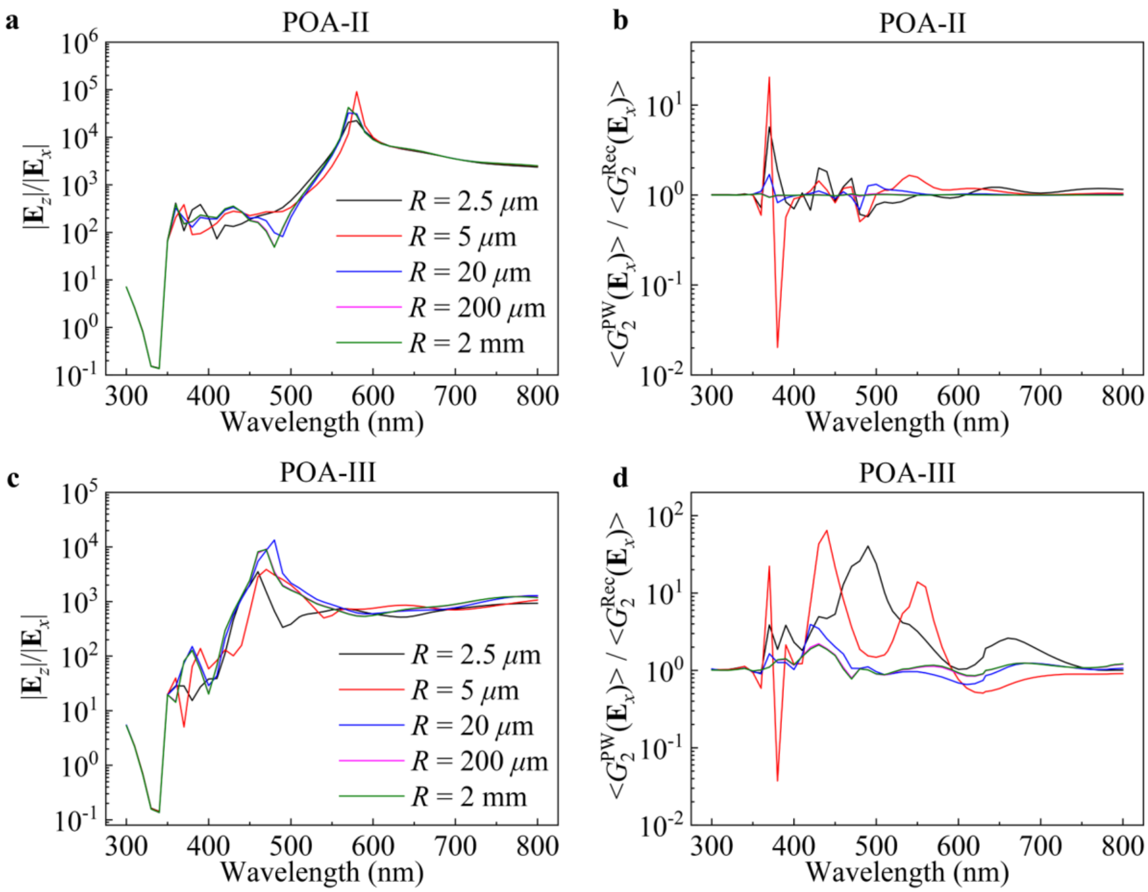

Figure S7. The ratio of $\left|\mathbf{E}_{\mathrm{far}}^{\mathrm{Exp}}\left(\mathbf{R},\mathbf{p}_{\mathrm{loc,z}}^{\mathrm{Exp}}(\mathbf{r}_{\mathrm{m}})\right)\right| / \left|\mathbf{E}_{\mathrm{far}}^{\mathrm{Exp}}\left(\mathbf{R},\mathbf{p}_{\mathrm{loc,x}}^{\mathrm{Exp}}(\mathbf{r}_{\mathrm{m}})\right)\right|$ in the $\mathbf{p}_{\mathrm{loc,z/x}}^{\mathrm{Exp}}$ couple with POA-II (a), and with POA-III (c). The wavelength-dependent ratios of the averaged radiation enhancement factors $\langle G_2^{\mathrm{PW}}\rangle/\langle G_2^{\mathrm{Rec}}\rangle$ in the POA-II-$\mathbf{p}_{\mathrm{loc,x}}^{\mathrm{Exp}}$ system (b) and in the POA-III-$\mathbf{p}_{\mathrm{loc,x}}^{\mathrm{Exp}}$ system (d). $\left|\mathbf{E}_{\mathrm{far}}^{\mathrm{Exp}}\left(\mathbf{R},\mathbf{p}_{\mathrm{loc,z}}^{\mathrm{Exp}}(\mathbf{r}_{\mathrm{m}})\right)\right| / \left|\mathbf{E}_{\mathrm{far}}^{\mathrm{Exp}}\left(\mathbf{R},\mathbf{p}_{\mathrm{loc,x}}^{\mathrm{Exp}}(\mathbf{r}_{\mathrm{m}})\right)\right|$ is indirectly calculated by directly calculating $\left|\mathbf{E}_{\mathrm{loc,z}}^{\mathrm{Rec}}\left(\mathbf{r}_{\mathrm{m}},\mathbf{p}_{\mathrm{far}}^{\mathrm{Rec}}(\mathbf{R})\right)\right| / \left|\mathbf{E}_{\mathrm{loc,x}}^{\mathrm{Rec}}\left(\mathbf{r}_{\mathrm{m}},\mathbf{p}_{\mathrm{far}}^{\mathrm{Rec}}(\mathbf{R})\right)\right|$ by solving Maxwell's equations only once at a wavelength according to the rigorous ORT.

SI 10. Near-field modes in scanning probe-substrate coupling system (POA-III)

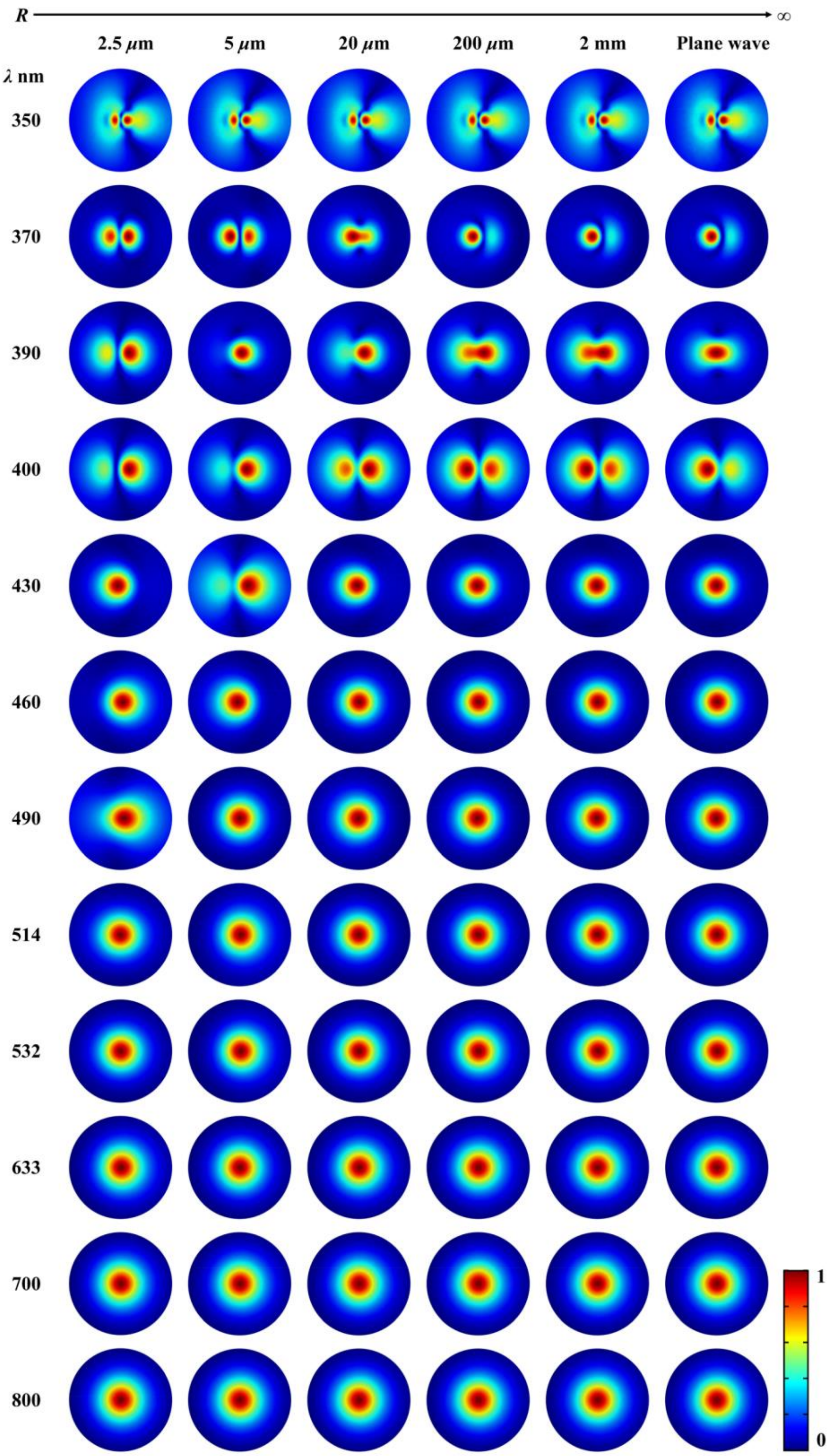

Figure S8. Near-field modes ($|\mathbf{E}_z|/|\mathbf{E}_{z,max}|$) in the POA-III system excited by an oscillating electric dipole and a PW at different wavelengths λ. The projection area (diameter is 50 nm) is located 1 nm above the surface of the substrate under a tip.

REFERENCES

1. Landau, L. D.; Lifchitz, E. M.; Pitaevskii, L. P. *Electrodynamics of Continuous Media*, 2nd ed.; Pergamon Press: Oxford, 1984.

2. Le Ru, E. C.; Etchegoin, P. G. *Principles of Surface Enhanced Raman Spectroscopy and Related Plasmonic Effects*; Elsevier: Amsterdam, 2009.

3. Novotny, L.; Hecht, B. *Principles of Nano-Optics*, 2nd ed.; Cambridge University Press: Cambridge, 2012.

4. Jackson, J. D. *Classical Electrodynamics*, 3rd ed.; Wiley: Berlin, 1998.